Groundwater Monitoring&Remediation

Research Article

Complementary Field and Laboratory Batch Studies to Quantify Generation Rates of Perfluoroalkyl Acids in a Contaminated Agricultural Topsoil with Unknown Precursors

by Alexander Arthur Haluska, Klaus Röhler, Joel Fabregat-Palau, Diogo A. M. Alexandrino, Sergey Abramov, Katharine J. Thompson, Daniel Straub, Sara Kleindienst, Boris Bugsel, Jonathan Zweigle, Christian Zwiener and Peter Grathwohl

Abstract

Soil microbiome changes and generation rates of per- and polyfluoroalkyl substances (PFAS) precursors were studied in a contaminated agricultural field using a combination of field and laboratory batch microcosm studies. 16S rRNA gene amplicon sequencing was used to track how microbial community composition changed over time, while perfluoroalkyl acids (PFAA) generation rates were quantified using a combination of field and batch incubations combined with the direct total oxidizable precursor (dTOP) assay. The study site in Brilon-Scharfenberg, North Rhine-Westphalia, Germany, has PFAS contamination in the topsoil (0 to 30 cm) originating from compost. Generation rate constants of these short-chain PFAA estimated from batch incubations (0.12 to 0.75 1/year) were higher but similar to rate constants from the fields (0.05 to 0.22 1/year). Long-term field mass discharge data (2009 to 2023) suggest that at least 60 years are needed to remove 99.99% of short-chain PFAA and their precursors. 16S rRNA gene amplicon sequencing data revealed a major impact of PFAA on the biodiversity of soil microorganisms, with batch-incubated contaminated soils showing higher richness and diversity indexes than field control soils. However, most of these impacts occurred at lower taxonomical ranks and did not seem to have a prominent impact on the overall structure of the autochtonous microbial communities of the soils where PFAA were produced and accumulated. Overall, our findings demonstrate that well-controlled aerobic batch test combined with the results of dTOP assay are a suitable approach for estimating short-chain PFAA generation rates. Additionally, our research suggests that the complete removal of PFAA precursors from topsoil will take decades.

Introduction

Agricultural soils have recently been identified as a major source of per- and polyfluoroalkyl substances (PFAS) contamination in groundwater, largely due to the application of compost/biosolid mixtures on topsoil (Sepulvado et al. 2011; Guelfo and Higgins 2013; Bugsel and Zwiener 2020; Johnson 2022; Munoz et al. 2022). These sites pose a long-term challenge as the complex behavior of multiple constituents in both the vadose zone and groundwater can be difficult to resolve, especially if the total PFAS reservoir is unknown (Röhler et al. 2021). Furthermore, topsoil (0 to 30 cm) can be a long-term source (i.e., decades) of perfluoroalkyl acids (PFAA) due to ongoing transformation of PFAA precursors (e.g., dialkyl phosphate esters) that are retained in topsoil because of their generally strong sorption behaviors (McLachlan et al. 2019; Silva et al. 2019; Fabregat-Palau et al. 2021). These PFAA precursors are susceptible to biotransformation, under both oxic and anxoic conditions, leading to more mobile PFAA (Wang et al. 2009; Liou et al. 2010; Wang et al. 2011; Wang et al. 2012; Liu and Avendano 2013; Huang and Jaffe 2019; Chen et al. 2020; Che et al. 2021; Newell et al. 2021; Nickerson et al. 2021). Short-chain PFAA, such as perfluoroalkyl carboxylic acids (PFCA) with less than seven fluorinated carbons and perfluoroalkyl sulfonic acids (PFSA) with less than six fluorinated carbons atoms, may then be mobilized from the topsoil to groundwater due to leaching by seepage water (Anderson 2021; Bekele et al. 2020; Rayner et al. 2022).

Of particular concern in shallow PFAS contaminated agricultural soils is the aerobic biotransformation of precursors to PFAA (Fang et al. 2020; Sharifan et al. 2021; Schaefer et al. 2022). This transformation process appears to be a co-metabolic, multi-step process that certain

doi: 10.1111/gwmr.12680

PFAS-tolerant microorganisms (e.g., *Pseudomonas aeruginosa* HJ4 and *Gordonia* sp.) can carry out (D'Eon and Mabury 2007; Rhoads et al. 2008; Wang et al. 2009; Lewis et al. 2016; Weathers et al. 2016; Yi et al. 2016; Yi et al. 2019). However, there is limited knowledge about the impact that PFAS compounds have on the soil microbial community structure.

Obtaining reliable estimates for PFAA generation rates is critical for estimating remediation time scales at contaminated sites (Yoo et al. 2010; Röhler et al. 2023). Since precursor types and their concentrations are often unknown, bulk PFAA generation rates can be estimated using field and laboratory methods that track concentration changes of final precursor transformation products. However, determining trends can be complicated by seasonality and nonuniform distribution of contaminants at a site (Naidu et al. 2012). Field measurements cannot distinguish between microbial and abiotic processes. Batch incubations, though common, often result in quicker generation rates than observed in the field due to "optimal conditions" (Benskin et al. 2013; Liu and Liu 2016; Haluska and Finneran 2021; Sharifan et al. 2021; Schaefer et al. 2022; Röhler et al. 2023).

Only a few studies have characterized the extent of PFAS contamination and generation of PFAA at agricultural sites (Washington et al. 2010; Yoo et al. 2010; Stahl et al. 2013; Röhler et al. 2021; Schaefer et al. 2022; Röhler et al. 2023). Among them, Röhler et al. (2021) evaluated PFAS field leaching data from a time period between 2007 to 2019 from the same agricultural site studied here (Brilon-Scharfenberg, North Rhine-Westphalia, Germany). Their trend analysis (i.e., Seasonal-Kendall, Mann-Kendall, exponential decay) suggested leaching of PFAA would continue for decades. However, these time scale estimates exhibit high uncertainty as the precursor reservoir in the field was unknown at the time of application. To overcome these uncertainties, soil samples were collected at the site for batch incubations in combination with an extended analysis of field leaching data. Additionally, 16S rRNA gene amplicon sequencing analyses were conducted on contaminated soil samples from batch incubations at different time points and compared with a field control (i.e., no known application of PFAS) from an adjacent field. The objective of this study was to integrate field and batch studies to estimate short-chain PFAA generation rates in PFAS contaminated topsoil, while simultaneously characterizing the concomitant impact of the generation and accumulation of these PFAA on the soil microbiome.

Materials and Methods

Chemicals, Reagents, and Sterilization Processes

Details of the chemicals used in this study are provided in the Supporting Information (Section S2.1; Tables S1 to S3).

Study Site and Sample Collection

In 2006, the State Office for Nature, Environment, and Consumer Protection (LANUV) discovered that 10 ha of farmland in Brilon-Scharfenberg, North Rhine-Westphalia Site (BS-NRW), had been contaminated with PFAS. This site was identified as the primary source for PFAA found in the Ruhr and Möhne Rivers (Joerss et al. 2020). PFAS detected at BS-NRW site was due to repeated application of PFAS-containing compost from 2004 to 2006, leading to topsoil contamination. To mitigate PFAS discharge into the adjacent River Steinbecke, a drainage system connected to an activated carbon filtration plant was installed in early 2007. Since then, perfluorooctanoic acid (PFOA) and perfluorooctanesulfonic acid (PFOS) inflow concentrations into the activated carbon filtration plant have been continuously monitored. In 2008, perfluorobutanoic acid (PFBA), perfluoropentanoic acid (PFPeA), perfluorohexanoic acid (PFHxA), perfluoheptanoic acid (PFHpA), perfluorononanoic acid (PFNA), perfluorodecanoic acid (PFDA), perfluorobutanesulfonic acid (PFBS), and perfluorohexanesulfonic acid (PFHxS) were added to the monitoring program; perfluoroundecanoic acid (PFUnA), perfluorododecanoic acid (PFDoA), and perfluorodecane sulfonic acid were included in 2017.

While the specific classes of PFAS present in the compost were unknown at the time of application, a recent nontargeted analysis by Zweigle et al. (2023) of a homogenized composite sample (also used in batch incubations) identified multiple classes of compounds, including PFCA, PFSA, pentafluorosulfanyl perfluoroalkyl sulfonic acids (SF_5-PFSA), unsaturated perfluoroalkyl sulfonic acids (U-PFSA), unsaturated pentafluorosulfanyl sulfonic acids (U-SF_5-PFSA), ether perfluoroalkyl sulfonic acids (ether-PFSA), unsaturated ether perfluoroalkyl sulfonic acids (U-ether-PFSA), di-unsaturated perfluoroalkyl sulfonic acids (di-U-PFSA), unsaturated ether pentafluorosulfanyl perfluoroalkyl sulfonic acids (U-ether-SF_5-PFSA), H-perfluoroalkyl sulfonic acids (H-PFSA), di-unsaturated ether PFSA, and ether perfluoroalkyl carboxylic acids (ether-PFCA). The detection of these different compounds suggests that a mixed industrial waste was applied to the field (Zweigle et al. 2023).

Topsoil at the BS-NRW site was sampled in October 2021 (Section S2.2; Figure S1). Six-different zones on the north side of the BS-NRW contaminated field site were sampled because the north site was thought to be less depleted of precursors (i.e., 537 to 1400 µg/kg C_4-C_{10} PFAA from topsoil cores in 2019) due to the absence of agricultural activity since the discovery of PFAS contamination in 2006. In contrast, the south site has experienced active agricultural activity since 2006 and showed lower concentration of PFAS remaining in topsoil (i.e., 75 to 1810 µg/kg C_4-C_{10} PFAA from topsoil cores in 2019) (Schroers 2021). A field control sample (i.e., PFAS-free soil) was also taken from an adjacent site with no known application of PFAS compost but similar historical farming practices, to serve as a quality control and for baseline for microbial community comparison.

All topsoil was sampled using an Edelmann auger in a diagonal grid with 20 m spacing to a depth of 30 cm. Sterilization procedures of field equipment are detailed in Section S2.3. For contaminated samples, mixing was conducted in two stages. First, samples from each zone were homogenized using a riffle bank (Section S2.4; Figure S2). Then, 2 kg of homogenized soil from each zone was mixed again

using a riffle bank to obtain a composite sample, which was then sieved to less than 2 mm. The same mixing process was repeated for the field control sample. The contaminated sample was subsequently subsampled for soil physiochemical analysis (e.g., soil pH, total organic carbon (TOC), and cation exchange capacity (CEC)), microbial analysis, and the non-targeted analysis as previously summarized. The composite sample was used for batch incubation as described later. The TOC of the contaminated composite sample was determined to be 3.7%, the soil pH was 6.7, and the CEC was 23 $cmol^+$/kg (Section S2.4; Table S4).

Soil Extraction

The composite, PFAS-contaminated topsoil was extracted with methanol (MeOH) and analyzed for C_4-C_{12} PFCA and C_4-C_{10} PFSA to determine the amount of PFAA present at the time of sampling. Soil extraction was conducted as described by Röhler et al. (2023). Briefly, 50 g of soil was dried in an oven at 40 °C and then pulverized and homogenized using a ball mill. Then, 0.5 g of pulverized soil was placed in 15 mL polypropylene (PP) centrifuge tubes and extracted using 5 mL of MeOH. Next, the suspension was vortexed for 10 s, sonicated for 30 min, and then put shaken at 220 rpm for 30 min. The 15 mL PP tubes were then centrifuged at 7,000 rcf for 15 min and the supernatant was transferred to a 12 mL glass vial. The extraction was repeated, and the extracts were combined and evaporated under a gentle stream of nitrogen at 40 °C until dryness. The samples were then reconstituted in 1 mL of a MeOH/water (1:1, v/v) solution. Internal standards prepared in MeOH were spiked into the reconstituted sample by the ultra performance liquid chromatograph (UPLC) autosampler before injection to account for matrix and ionization effects. Results from recovery experiments, as described in Section S2.5 and previously reported by Röhler et al. (2023), showed recoveries greater than 85%.

Direct Total Oxidizable Precursor (dTOP) Assay

The PFAA precursor reservoir was quantified using the direct total oxidizable precursor (dTOP) assay as described by Göckener et al. (2022). To quantify the total PFAS reservoir, 0.1 g of soil subsamples (done in triplicate) from the composite, contaminated sample were weighed into 100 mL Schott bottles and 100 µL of methanolic internal standard (100 µg/L) solution was added to each subsample; Then, 100 mL of a 0.5 M NaOH and 0.2 M $K_2S_2O_8$ solution was added to each subsample, and the bottles were placed in an oven at 85 °C for 7 h and shaken frequently by hand. After the samples cooled to room temperature, the pH was adjusted to 6.0 ± 0.5 using HCl. The aqueous solutions from each subsample were then enriched using solid phase extraction (SPE) cartridges (Chromabond HR-XAW, 3 mL, 200 mg, Machery-Nagel). All cartridges were pre-conditioned with 6 mL of 0.1% NH_4OH in MeOH, 3 mL of MeOH, and 6 mL of water. The samples were passed through the cartridges using a vacuum at an approximate rate of 1 drop/s. Afterward, the cartridges were washed with 6 mL of water and dried. Elution was achieved with 3 mL MeOH and 6 mL of 0.1% NH_4OH in MeOH. The extracts were evaporated under a gentle stream of nitrogen at 40 °C until dryness and reconstituted in 1 mL MeOH/water (1:1, v/v). All dTOP assays were done in triplicate. Results from the recovery tests, as described in Section S2.5 and previously reported by Röhler et al. (2023) showed recoveries greater than 75% for C_4-C_{10} PFCA and C_4-C_9 PFSA.

Column Leaching Tests

Up-flow column leaching tests, conducted in accordance with German DIN 19528, were used to pre-treat the contaminated soil. This step was intended to remove existing short-chain PFAA, creating a baseline for accurately monitoring their subsequent generation from PFAA precursors in the following incubation tests (DIN Media Gmbh 2009; Röhler et al. 2023). The columns had a diameter of 5 cm and a length of 30 cm. The soil was packed into the columns between two 2 cm thick acid washed quartz layers (grain size 0.6 to 1.2 mm, Gebrüder Dorfner GmbH & Co, Hirschau Germany) to ensure uniform flow across the column. The columns were flooded from the bottom to the top within 2 h, then the flow rate was adjusted to ensure a contact time of 5 h. Columns were leached until specific liquid-to-solid (*LS*, L^3/M) ratios were reached, including 0.1, 0.3, 1, 2, 4, and 10 L/kg. After *LS* 10, the soil was collected, homogenized in a stainless-steel bowl and used in soil batch incubations as later described. The *LS* ratio can be converted into time (*t*), as described by Grathwohl and Susset (2009) and Röhler et al. (2023):

$$t = \frac{LSx\rho}{vn} \qquad (1)$$

where x is the length of the column (L); v is the seepage velocity (L/T); ρ is the dry bulk density (M/L^3); and n is the porosity (–). Control columns containing only quartz sand were set up and run in parallel to columns with PFAS-contaminated topsoil to check for any background contamination. The column eluates were stored at 4 °C until further analysis.

The sample preparation procedure for aqueous samples, both those requiring and not requiring SPE cartridges, are described in Section S2.6. Note that SPE cartridges were used for aqueous samples when PFAS levels resulting from direct dilution were below the limits of quantification (LOQ) levels (as detailed in Section S2.7). Results from a recovery experiment for aqueous samples showed greater than 80% recovery for all PFAS, except for PFDoA, which had a recovery of 76% (Section S2.6; Table S6) (Röhler et al. 2023). As discussed in the results section, column leaching tests were not applied to the field control soil, as dTOP and target analysis showed low amounts of PFAS (less than 0.70 µg/kg).

Soil Batch Incubations

Soil incubations were constructed using the contaminated topsoil after leaching to remove short-chain PFAA. Briefly, 350 g of water-saturated topsoil material and 1 L of autoclaved deionized water were placed into 2 L (nominal) glass bottles and sealed under atmospheric headspace (*LS* = 2.86 L/kg). To facilitate mixing, the incubations were placed on a horizontal shaker table at 160 rpm in a dark room

maintained at 20 °C. To maintain oxic conditions, the bottles were regularly opened under sterile conditions. Oxygen (O_2) levels in the aqueous phase were tracked using a Fibox 3 Minisensor Oxygen Meter from PreSens (Regensburg, Germany). Electrical conductivity and pH were monitored using laboratory probes (SCHOTT® Instruments). Sterile controls were set up in the same way as the contaminated batch incubation but autoclaved at 121 °C for 60 min for three consecutive days. After samples were autoclaved, they were dosed with an antibiotic mixture (i.e., kanamycin, chloramphenicol, and cycloheximide) that resulted in a final concentration of 100 mg/L of each antibiotic to further inhibit microbial or enzymatic activities (Liu et al. 2010). Field controls were set up in the same way as the experimental contaminated batch incubations. All experiments were conducted in triplicate.

At each sampling point, an aliquot of 18 to 20 mL was collected (controlled by weight), centrifuged at 7,000 rcf for 15 min, transferred to a 2-mL Eppendorf tube, and centrifuged again at 20,000 rcf for 15 min. The supernatant was then diluted with MeOH (final composition water/MeOH 1:1 v:v) and stored at 4 °C until analyses by UPLC using a mass spectrometer (MS/MS) detector. If PFAS were found at levels below LOQ, the supernatant was enriched using an SPE cartridge as detailed in Section S2.6. Additionally, solid-phase samples for microbial analysis were collected at 0, 28 and 60 d using sterilized 2 mL Eppendorf tubes. Each microbial sample was centrifuged at 10,600 rcf for 15 min before being stored at −20 °C.

Instrument Analysis for Laboratory Data

Details on the instrumental analysis (i.e., UPLC and MS/MS systems used, source parameters and MS acquisition, as well as LOQ) are provided Section S2.7 (Tables S7 to S9). PFAS analyzed in batch incubations included PFBA, PFPeA, PFHxA, PFHpA, PFOA, PFNA, PFDA, PFUnA, PFDoA, PFBS, perfluoropentane sulfonic acid (PFPeS), PFHxS, perfluoroheptane sulfonic acid (PFHpS), PFOS, perfluorononanesulfonic acid (PFNS) and PFDS.

Field Monitoring Data

Field data collected from August 2009 to August 2023 included PFAA concentrations, referred to as generation product concentrations (C_{GP}, M/M), and volumetric water flow rates (Q, L^3/T). The data were obtained from sampling the seepage water in the drainage basin and were used to determine cumulative masses of PFAA. Aqueous samples were screened for PFAS by the LANUV laboratory via UPLC–MS/MS, as previously described elsewhere (Röhler et al. 2021). Aqueous samples were screened for PFBA, PFPeA, PFHxA, PFHpA, PFOA, PFNA, PFDA, PFUnA, PFDoA, PFBS, PFHxS, PFOS, and PFDS. The LANUV started monitoring these PFAS at different times, as discussed earlier in the site history. Note that this data extends the field observations described by Röhler et al. (2021), which only included data up to 2019.

Time Scales for PFAA Generation for Batch and Field Data

To determine the time scales, a simple exponential source decay model was used to describe the decrease in the unknown PFAA precursors concentration (C_{PC}) per mass of soil solid (M/M, e.g., by µg/kg) as previously described by Röhler et al. (2023):

$$C_{PC} = C_{PC,0}\exp(-\lambda\, t) \tag{2}$$

where $C_{PC,0}$ denotes the initial concentration of precursors in the topsoil per mass of soil solid (M/M); and λ is a rate constant (1/T). Thus, the decrease in C_{PC} in the topsoil is proportional to an increase in the relative C_{GP} with time:

$$C_{GP} = C_{GP,\infty}(1-\exp(-\lambda\, t)) \tag{3}$$

where $C_{GP,\infty}$ denotes the final yield of generation product (i.e., total conversion of $C_{PC,0}$) per mass of soil solids. For short time periods (i.e., negligible precursor depletion) this reduces to a linear approximation:

$$C_{GP} = C_{GP,\infty}\ \lambda\, t \tag{4}$$

where the term $C_{GP,\infty}\ \lambda$ denotes the initial generation rate (M/M/T) when depletion of the precursor still is negligible, indicating a linear increase in C_{GP} for short-term laboratory batch tests (e.g., 60 d incubation period). The unknown $C_{GP,\infty}$ may be estimated by the dTOP assay soil concentration (C_{dTOP}, M/M), meaning that λ can be determined by:

$$\lambda = \frac{C_{GP}}{C_{\mathrm{dTOP}} \times t} = \frac{G}{C_{\mathrm{dTOP}}} \tag{5}$$

where G denotes the generation rate (M/M/T) of generated products from precursors (=C_{GP}/t). Mean values of G were determined from triplicate batch incubation using the Microsoft Excel® regression tool package.

For longer time periods (i.e., field scale), Q measurements coupled with individual C_{GP} levels produce temporal fluxes of generation product (F_{GP}) (M/T) (also known as a mass rate), allowing for the determination of the cumulative mass of a generation product (M_{GP}) produced during the transformation of PFAS precursors as detailed:

$$M_{GP} = \sum_{i}^{\infty} C_{GP}\, Q_i\, \Delta t_i = \int_0^t F_{GP}\, dt = M_{\infty}\left[1-\exp(-\lambda\, t)\right] \tag{6}$$

where t is the time period of generation (T); M_{∞} (=F_{GP}/λ) is the total mass of generation products that can theoretically be generated from precursors in the topsoil. Equation 6 was fit to the field data by treating M_{∞} and λ as fitting parameters to minimize the difference between the model and the field data. M_{∞} and λ were determined using the BoxLucas1 model in OriginPro® 2024. Lab derived rate constants (Equation 5) may be compared to the field-derived rate constants (Equation 6).

16S rRNA Gene Amplicon Sequencing and Bioinformatics Analysis

To evaluate the impact of PFAA generation and/or accumulation on the soil microbial community under controlled conditions, batch samples were collected at 0, 28, and 60 d,

in both PFAS-free and contaminated conditions, DNA was extracted and submitted for 16S rRNA gene amplicon sequencing. Total genomic DNA was isolated using the PowerSoil DNA Isolation Kit (MO BIO Laboratories, Carlsbad, CA, USA). DNA concentration and quality were assessed using a NanoDrop 2000 spectrophotometer (ThermoFisher Scientific, Ottawa, Canada) (O'Carroll et al. 2020). The 16S rRNA gene was amplified using primers 515F and 806R targeting the V4 region (Caporaso et al. 2010). Library preparation (Nextera, Illumina) and 250 bp paired-end sequencing with MiSeq (Illumina, San Diego, USA) using v2 chemistry were performed by Microsynth AG (Switzerland), and between 70,222 and 162,259 read pairs were obtained for each sample.

Sequencing data were analyzed with nf-core/ampliseq v2.4.0, which includes all analysis steps and software and is publicly available (Ewels et al. 2020; Straub et al. 2020), with Nextflow v22.04.5 (Di Tommaso et al. 2017) and singularity v3.8.7 (Kurtzer et al. 2017). Nf-core/ampliseq was executed with parameters "–FW_primer GTGYCAGCMGCCGCGGTAA –RV_primer GGACTACNVGGGTWTCTAAT –trunc_qmin 35 –dada_ref_taxonomy silva=138 –picrust –sample_inference pooled." Primers were trimmed, and untrimmed sequences were discarded (less than 10% per sample), with Cutadapt version 3.4 (Martin 2011). Adapter and primer-free sequences were processed as one pool with DADA2 v1.22.0 (Callahan et al. 2016) to eliminate PhiX contamination, trim reads (before median quality dropped below 35; forward reads were trimmed at 230 bp and reverse reads at 167 bp), correct errors, merge read pairs, and remove polymerase chain reaction (PCR) chimeras; ultimately, 11,516 amplicon sequencing variants (ASVs) were obtained across all samples. Taxonomic classification was performed with DADA2 and the SILVA v138 database (Pruesse et al. 2007). The taxonomically annotated datasets were then further curated using the *phyloseq* package in R environment (v.4.3.2) (Holmes and McMurdie 2013).

First, ASVs taxonomically classified as non-bacterial or -archael taxa (e.g., "Eukaryota," "Chloroplast," and "Mitochondria") were filtered out of the dataset and a relative abundance threshold of 1% was applied. Then, to assess the diversity of each experimental condition, the alpha-diversity descriptors "Observed," "Chao1" and "Shannon" were calculated for each sample. To estimate the divergence of the microbial communities among the different conditions and incubation periods (i.e., beta-diversity analyses), Bray-Curtis distances were determined and visualized in a Non-Metric Multidimensional Scaling (NMDS) plot.

Additionally, enrichment and correlation analyses were performed using the *microbiomemarker* (Cao et al. 2022) and *corrplot* (Wei 2021) R packages, respectively. To improve the fidelity of these quantitative analyses, the filtered ASV datasets were further curated by excluding ASVs only present in one replicate per condition. Then, a Linear Discriminant Effect Size Analysis (LEfSe) was implemented to determine the ASVs enriched in the field control and contaminated batch incubations, with a linear discriminant analysis (LDA) score cutoff of 3.5, of which only those displaying significance levels below 1.0×10^{-3} were considered. Finally, correlations between the predominant bacterial or archaeal ASVs present in the contaminated batch samples across all incubation periods, PFAA concentrations and physicochemical parameters (O_2, conductivity and pH) were calculated using the Spearman's rank correlation coefficients, considering only significant correlations ($p < 0.001$). Note that a downloadable Excel® file with the meta data and the ASVs is provided (Dataset S1). All the obtained sequences were deposited into National Center for Biotechnology Information under the BioProject accession number PRJNA894146 (https://www.ncbi.nlm.nih.gov/bioproject/PRJNA894146).

Results and Discussion

PFAA and Precursor Concentrations in Soil

Targeted PFAS analyses in the BS-NRW contaminated soil identified PFOA, PFOS, PFNS, and PFDS as the major contaminants, accounting for 98% of PFAA analyzed (Figure 1), with concentrations of 75, 225, 227, and 592 µg/kg, respectively. Other C_4-C_7 and C_9-C_{12} PFCA, PFBS, and PFHxS levels ranged from 0.6 to 4.2 µg/kg. The high concentrations of PFOA and PFOS in the topsoil may explain their higher abundance (up to 75%) in the monitored seepage

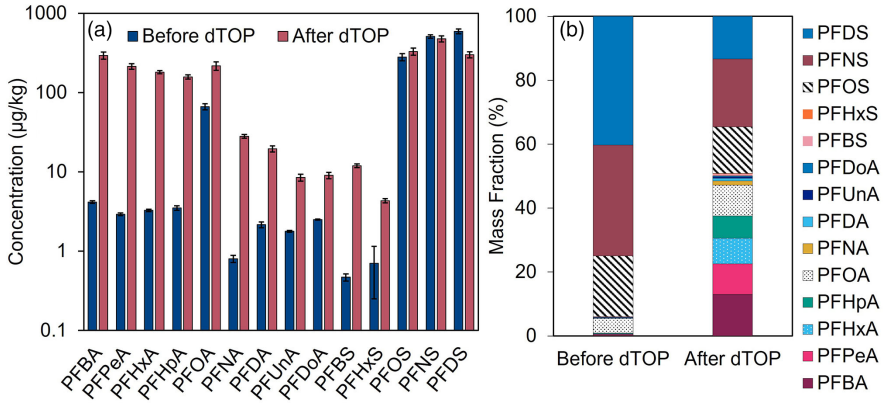

Figure 1. (a) Mean concentration (µg/kg) of perfluoroalkyl acids (PFAA) detected by targeted analysis before and after the direct total oxidizable precursor (dTOP) assay; error bars indicate standard deviation; (b) Mass fraction (%) of PFAA detected in the contaminated topsoil sample before and after the dTOP assay.

water and their continuous leaching to groundwater (Röhler et al. 2021). Blank soil extractions taken from a PFAS-free adjacent site (field control samples) were analyzed in parallel to assess PFAS levels. The total concentration of extractable C_4-C_{12} PFCA and C_4-C_{10} PFSA in the contaminated soil was 1470 µg/kg (Figure 1), whereas it was less than 0.70 µg/kg (i.e., 0.3 µg PFOA/kg; 0.4 µg PFOS/kg) in the field control samples.

The dTOP assay results revealed an extensive reservoir of precursors that have the potential to be transformed to PFAA (Figure 1). Semiquantitative, non-targeted analyses had previously estimated that only approximately 3% of all identified PFAS in the soil could serve as potential PFAA precursors during dTOP, explaining about 41% of the PFAA that formed during the assay (Zweigle et al. 2023). Concentrations of short-chain PFCA increased up to a factor of 73 after oxidation process, while PFOA concentrations increased only threefold (Figure 1). Notably, PFBS and PFHxS concentrations were 20- and 6-fold higher, respectively, after dTOP. Although dTOP oxidation produces PFCA as end-products (Houtz and Sedlak 2012), the generation of several PFSA has also been reported, attributed to the base-catalyzed hydrolysis of perfluorosulfonamides (Cook et al. 2022) or the higher recovery of non-extractable PFSA during targeted analyses (Göckener et al. 2022). The presence of multiple polyfluorinated sulfonic acids in the original soil might have been precursors to perfluoroalkyl diacids detected after dTOP, potentially from unknown oxidation mechanisms (Zweigle et al. 2023). Potential precursors to PFSA were not identified, although they could also be present in this soil (Zweigle et al. 2023). PFOS and PFNS concentrations before and after dTOP had similar levels, suggesting that they were directly applied to the soil rather than being generated after precursor transformation. Conversely, PFDS concentrations were reduced by a factor of two, possibly due to strong sorption to soil solids in the aqueous setup of the dTOP assay.

Column Leaching Test

Figure 2 displays the leaching test results and reveals that short-chain PFCA were easily leached at low *LS* values, whereas relatively constant concentrations for long-chained PFAS were observed across the sampled *LS*, a typical behavior in leaching tests for contaminants with high sorption (Kabiri et al. 2022). Mass balance calculations using initial solid concentrations and cumulative PFAS mass in the different column eluates showed PFBA and PFPeA recoveries greater than 100% (Figure S3), which may indicate generation from PFAA precursors during the column test, as also observed by Braunig et al. (2019), or uncertainties in the analytical determination. Generally, the fraction of long-chain PFAA recovered in the column effluent decreases with increasing chain length, which may be attributed to their stronger sorption in solid particles (Fabregat-Palau et al. 2021). PFOA concentrations decreased by a factor of 10 but remained elevated (approximately 1 µg/L) after reaching *LS* 10. PFDoA effluent concentrations were less than LOQ in all cases, and PFPeS and PFHpS were less than 0.05 µg/L.

Soil Batch Tests

Laboratory batch incubations with contaminated topsoil (after column leaching treatment to remove short-chain PFAA) were conducted under aerobic conditions to derive generation rates for PFAA, as similarly performed elsewhere (Röhler et al. 2023). O_2 measurements demonstrated that oxic conditions were maintained (Table S10). pH values were maintained among the individual bottles, whereas conductivity increased over time.

Contaminated batch incubations showed linear increases of the mean aqueous concentrations for PFBA, PFPeA, PFHxA, PFHpA, PFOA, and PFBS over the 60 d tests (Figure 3). PFBA increased from 0.07 to 2.3 µg/L after 60 d, whereas PFPeA increased from 0.06 to 1.53 µg/L. PFHxA increased from 0.08 to 1.61 µg/L after 60 d, with a similar rise for PFHpA, where levels increased from 0.13 to 1.6 µg/L after 60 d. PFOA showed the greatest increase in concentration with levels rising from 0.86 to 10.4 µg/L after 60 d. PFBS showed the smallest increase in concentration with levels rising from 0.01 to 0.38 µg/L after 60 d. In contrast, long-chain PFAS did not show a significant concentration increase over time in the contaminated batch incubation (Section S3; Figure S4). This may indicate that transformation of parent precursors did not occur, or that the stronger tendency of long-chain PFAS to sorb into soil particles and the lower bioavailability of high molecular mass precursors may require longer experimental times to observe a significant increase of long-chain PFAS in solution (Fabregat-Palau et al. 2021; Fabregat-Palau et al. 2022). The field control showed PFAA values mostly less than

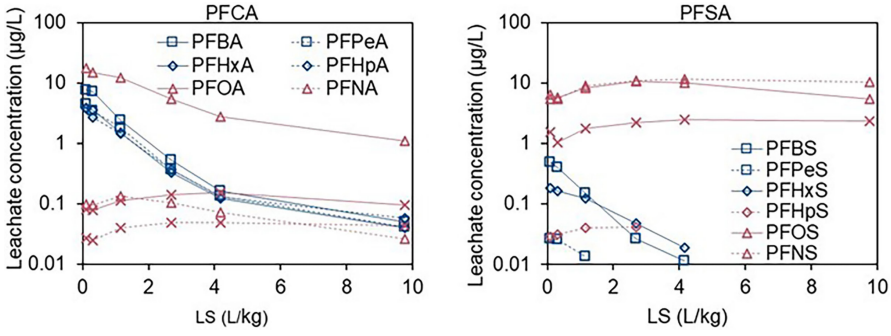

Figure 2. PFCA and PFSA concentration (µg/L) changes in saturated column leaching tests conducted with contaminated topsoil.

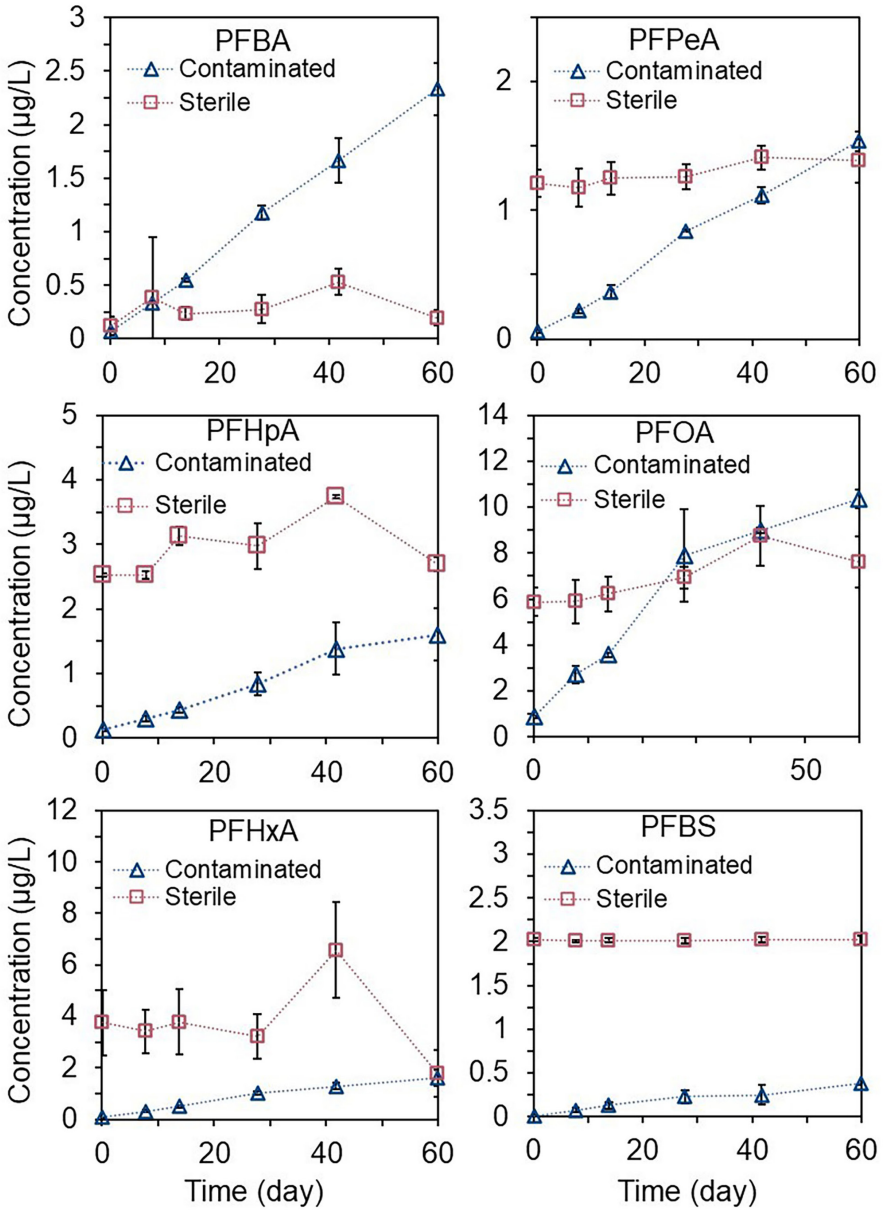

Figure 3. Mean aqueous concentration (µg/L) of C_4-C_9 PFAA for the contaminated topsoil (0 to 30 cm) in contaminated batch incubations and sterile controls; error bars indicate standard deviations from triplicates.

LOQ across the experiment, with no significant ($p>0.05$) increase across the experiment (data not shown). Similarly, sterile controls showed no significant ($p>0.05$) generation of PFAA during the duration of the experiment (Figure 3). However, the sterile controls showed higher initial concentrations of all PFAA already at the start of batch incubations (Figure 3 and Figure S4), likely due to the breakdown of PFAS precursors or soil organic matter when the topsoil was autoclaved; the latter may have resulted in a higher initial release of PFAS that were likely sorbed in the soil organic fraction (Fabregat-Palau et al. 2021), as higher DOC contents in solution were observed (Otte et al. 2018). The result shown in Figure 3 are also normalized to dry mass of soil and are displayed in Section S3 (Figure S5).

The increase of PFAS concentrations in solution over time allows for the calculation of generation rates using the regression tool package in Microsoft Excel®. Generation rates of mass PFAA ranged from 0.016 to 0.44 µg/kg/d (Table 1; Figure S5). Using the dTOP concentration as a proxy for transformable PFAA precursors, PFAA generation rate constants ranged from 0.12 to 0.75 1/year (Table 1), with PFOA having the highest rate constant. Higher rate constants for PFOA have also been observed previously in other contaminated soils (Röhler et al. 2023). However, these rate constants must be considered as a result of superposition of transformations of original precursors and intermediate products under optimum conditions.

Assessment of PFAA Rates Constants Using Field Data

Selected polyfluorinated compounds identified by nontargeted screening (Zweigle et al. 2023), and especially dTOP assay data, confirmed the presence of short-chain PFAA precursors in the topsoil, suggesting that the PFAA leaching data observed in the field may be due to ongoing

Table 1

Mean Generation Rates (G) and Rate Constants ($\lambda = G/C_{dTOP}$) Derived for PFAS from Contaminated Batch-Incubations; Experiments Were Done in Triplicate with Display of 95% Confidence Intervals (CI); dTOP Measurements Were Done in Triplicate with Standard Deviation Displayed (SD)

	G (µg/kg/d)			C_{dTOP} (µg/kg)		
Analyte	Mean	CI	R^2 (–)	Mean	SD	λ (1/year)
PFBA	1.0×10^{-1}	$\pm 7.0 \times 10^{-3}$	0.98	293	30	0.13
PFPeA	6.8×10^{-2}	$\pm 5.0 \times 10^{-3}$	0.98	214	18	0.12
PFHxA	7.0×10^{-2}	$\pm 1.2 \times 10^{-2}$	0.91	181	0.10	0.14
PFHpA	7.1×10^{-2}	$\pm 1.7 \times 10^{-2}$	0.83	158	10	0.16
PFOA	4.4×10^{-1}	$\pm 1.1 \times 10^{-1}$	0.84	217	26	0.75
PFBS	1.6×10^{-2}	$\pm 5.0 \times 10^{-3}$	0.84	12	0.70	0.48

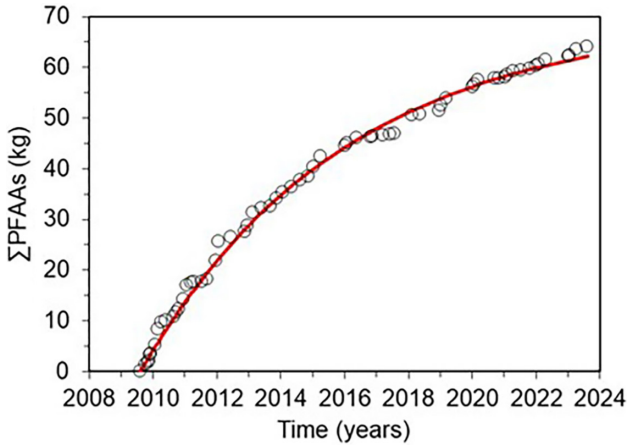

Figure 4. Cumulative mass (kg) of targeted perfluoroalkyl acids (ΣPFAA; i.e., PFOS, PFOA, PFBA, PFPeA, PFHxA, PFHpA, PFNA, PFDA, PFBS, and PFHxS) by sampling the seepage water in the drainage basin. Solid red line indicates fitted result of Equation 6.

PFAA generation processes. To assess the remaining potential of PFAA produced from precursors, the cumulative masses of transformation products were determined using PFAA mass rate data collected from 2009 to 2023. Figure 4 shows total cumulative PFAA masses, with M_∞ estimated to be 70 kg for the sum of all monitored PFAA (ΣPFAA). It should be noted that this is an extrapolation of Equation 6, which may be considered as a proxy for the potential mass of PFAA that can be produced from PFAS precursors in the topsoil. Table 2 shows individual and total cumulative PFAA masses (M_{total}), λ, M_∞, and coefficient of determination (R^2) obtained by fitting Equation 6. Individual cumulative mass PFAA curves are displayed in Figure S6. Although PFUnA, PFDoA, PFNS, and PFDS precursors were detected in soil extractions, they were not included in the analysis because monitoring of these compounds did not start until 2017.

The fitted λ for ΣPFAA was 0.16 (SE 0.0040)/year (Figure 4), indicating that it would take approximately 60 years to achieve 99.99% of M_∞ (i.e., depletion of remaining precursors that produce PFAA). While there is no discernible trend between short- and long-chain PFAA, individual λ parameters are listed in Table 2 and are within an order of magnitude of each other. Furthermore, these individual λ parameters are approximately within an order of magnitude to those reported by Röhler et al. (2021). Minor differences are likely due to the different time periods assessed for the field data. Unlike concentration data, stable water flow rate measurements were unavailable until January 2009. Furthermore, the data range selected started and ended in the same season to avoid bias caused by seasonal changes, as Röhler et al. (2021) showed that concentrations of the short-chain PFAS were higher in the fall and winter, suggesting generation and accumulation of these compounds during the spring and summer and mobilization during recharge in fall and winter. Overall, the data support the initial hypothesis that PFAA are continuously produced from precursors and that it will take decades until PFAA precursors have vanished from the contaminated site (Röhler et al. 2021).

Figure 5a compared λ parameters obtained from contaminated batch incubation experiments with field data. Laboratory λ parameters from this study for PFPeA and PFHxA were almost the same as the field λ parameters. PFBA field λ was almost twice as great as the laboratory λ parameter measured in this study, whereas the PFHpA laboratory λ was almost twice as great as the field λ. PFOA and PFBS contaminated batch incubation λ parameters were about six and four times greater than field λ parameters measured in this study, respectively. Taken together, these data imply that simple batch incubations may be a good basis for further development of laboratory tests needed for estimating PFAA generation in the field.

Figure 5b shows the mass distribution patterns detected in the aqueous phase during the 60 d batch incubations compared to cumulative field data from 2009 to 2023. The mass fraction of C_4-C_8 PFCA from the batch incubations shifted from 22% (day 0) to 82% (day 60) and is most likely caused by precursor transformation. Long-chain PFAS (e.g., PFOS, PFNS and PFDS) show no significant increase ($p > 0.05$) in contaminated batch incubations, although PFOS is one of the major contaminants found in the field. This suggests that long-chain PFSA are likely a combination of direct application of PFOS to the field (i.e., already present in the compost) and a potential reservoir of PFOS precursors as observed in Zweigle et al. (2023). Nonetheless, it could also be possible that transformation of high molecular weight PFSA precursors may be slower and could not be captured within the 60 d that the batch study was conducted.

Table 2

Individual Fitting Parameters for the Cumulative Mass of PFAA Measured from the Seepage Water in the Drainage Basin Using Data from August 2009 to August 2023; M_∞ and λ Were Determined with the LucasBox1 Model Using OriginPro® 2024; Standard Error (SE) Is Displayed for M_∞ and λ

PFAS Compound	M_∞ (kg)		λ (1/year)			
	Fitted Value	SE	Fitted Value	SE	R^2	$M_{Collected}$ (kg)
ΣPFAA	70	$\pm 8.5\times10^{-1}$	0.16	$\pm 4.0\times10^{-3}$	>0.99	64
PFBA	1.4	$\pm 3.5\times10^{-2}$	0.22	$\pm 1.7\times10^{-2}$	0.97	1.5
PFPeA	1.8	$\pm 3.2\times10^{-2}$	0.11	$\pm 3.1\times10^{-3}$	>0.99	1.4
PFHxA	2.6	$\pm 4.1\times10^{-2}$	0.12	$\pm 3.3\times10^{-3}$	>0.99	2.1
PFHpA	2.9	$\pm 5.8\times10^{-2}$	0.09	$\pm 2.8\times10^{-3}$	>0.99	2.1
PFOA	33	$\pm 4.8\times10^{-1}$	0.12	$\pm 3.2\times10^{-3}$	>0.99	27
PFNA	0.19	$\pm 1.7\times10^{-3}$	0.21	$\pm 4.7\times10^{-3}$	>0.99	0.19
PFDA	0.23	$\pm 4.3\times10^{-3}$	0.13	$\pm 4.9\times10^{-3}$	>0.99	0.20
PFBS	0.44	$\pm 6.4\times10^{-3}$	0.13	$\pm 3.5\times10^{-3}$	>0.99	0.38
PFOS	30	$\pm 3.0\times10^{-1}$	0.20	$\pm 5.1\times10^{-3}$	>0.99	29
PFHxS	0.34	$\pm 2.0\times10^{-2}$	0.05	$\pm 4.8\times10^{-3}$	>0.99	0.18

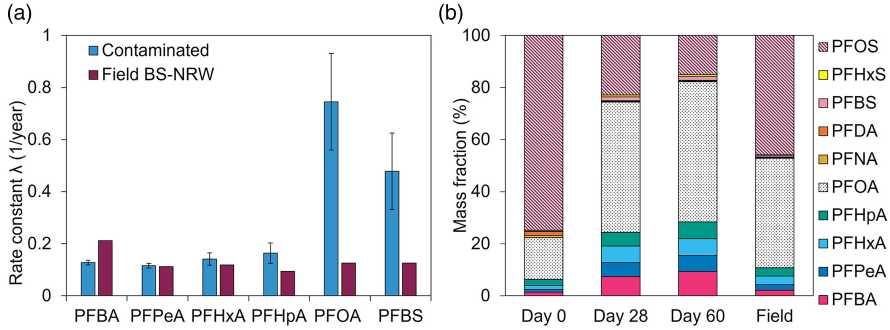

Figure 5. (a) Targeted perfluoroalkyl acids (PFAA) generation rate constants (λs, 1/yr) derived from contaminated batch incubation and from field cumulative masses calculated from August 2009 to August 2023. (b) Comparison of the average mass fraction (%) of PFAA in the aqueous phase during 60 d batch incubations and in the field at the end of the monitoring period; error bars indicate 95% confidence intervals of triplicate batch incubations.

Dynamics of the Soil Microbial Communities during the Batch Incubations

A temporal overview of the microbial community of field control and contaminated soils was obtained by 16S rRNA gene amplicon sequencing to observe the potential effects of PFAA generation and accumulation on soil microbiomes at different incubation intervals (0, 28, and 60 d). In general, contaminated batch samples consistently showed higher biodiversity indexes than field control samples, although both bacterial and archaeal richness (i.e., "Observed") and diversity descriptors (i.e., "Chao1" and "Shannon") decreased with the duration of the batch incubations (Section S3; Figure S7). These community dynamics were corroborated by the beta-diversity analysis, which showed a clear dissimilarity profile (based on the Bray-Curtis index) between field control and contaminated samples (Figure 6). It appears that the generation and accumulation of PFAA correlated with microbial community differentiation and therefore, potentially affected biodiversity. This observation is consistent with other reports showing increased microbial diversity profiles in soils or sediments exposed to various PFAS (Jiang et al. 2021; Wu et al. 2023). Still, PFAS exposure has also been known to negatively impact microbial community structure and diversity, particularly in soils with a lower content of organic carbon (Senevirathna et al. 2022). It is possible that higher contents of organic matter, which are known to contribute to a more stable and productive soil microbiota, can also improve microbial tolerance toward PFAS and even facilitate co-metabolic biotransformation of these recalcitrant substrates (Berhanu et al. 2023). Furthermore, the microbial community shifts observed between field control and contaminated samples in this study were more noticeable at lower taxonomical ranks, as they remained relatively stable between order and family level (Section S3; Figure S8). This supports the theory that, alongside the positive impact on bacterial biodiversity, soil function may not be significantly impacted by PFAA generation and/or accumulation, as the key func-

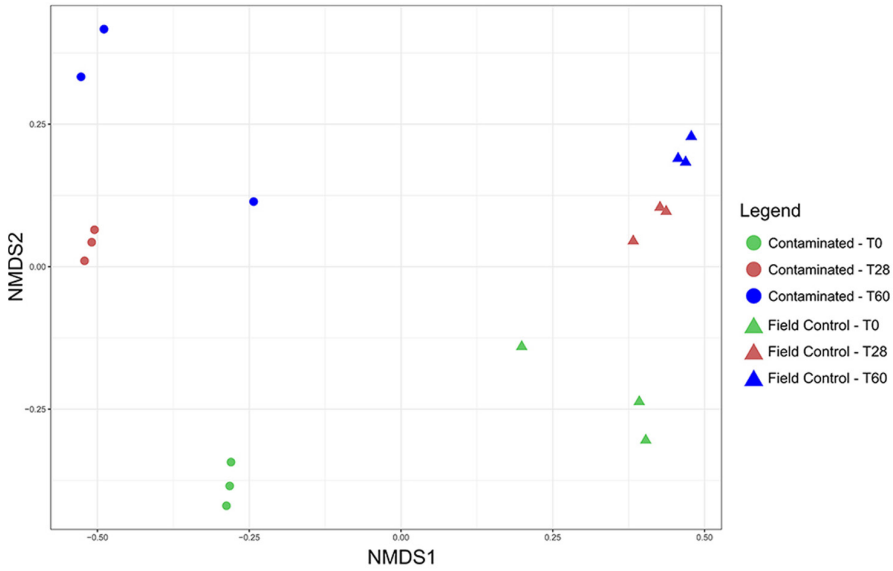

Figure 6. NMDS plot showing Bray-Curtis distances calculated between field control and contaminated samples at each sampling period (0, 28, and 60 d of incubation).

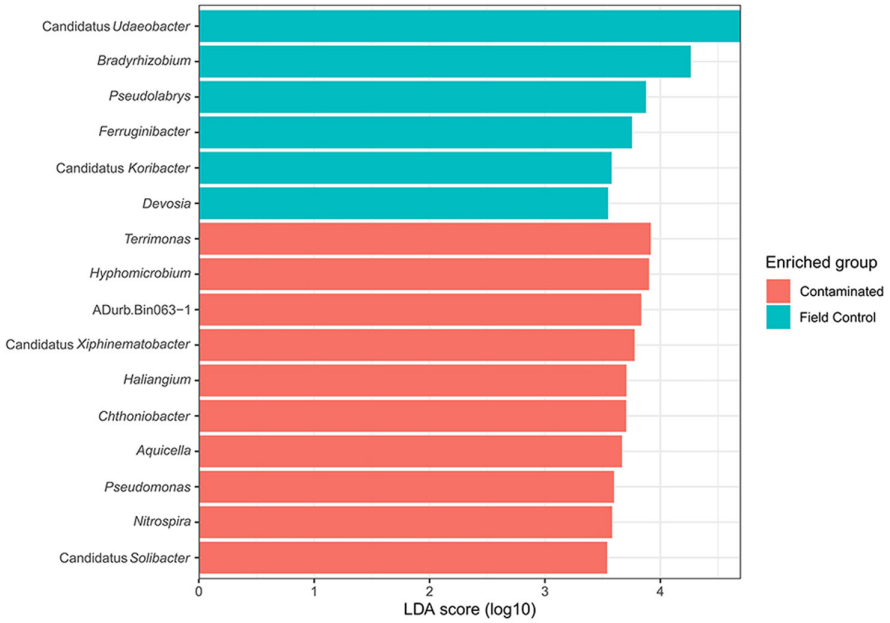

Figure 7. Taxonomical features specific to contaminated and field control samples, as determined by the LEfSe analysis (LDA score >3.5; $p < 0.001$).

tional microbial taxa remained coarsely similar regardless of the co-occurrence of different PFAA.

Clear shifts at the genus level were noticeable between field control and contaminated samples, so we performed enrichment and correlation analyses to better discriminate which genera were being selected under which experimental conditions. The LEfSe algorithm revealed a higher number of taxa (10 ASVs) being more affiliated with ($p < 0.001$) the contaminated samples than in the field controls (six ASVs) (Figure 7). However, these condition-specific ASVs are all affiliated with taxa known to participate in similar soil functions, namely carbon cycling (through polysaccharide degradation or carbon fixation), nitrogen fixation and nitrification. This suggests a potential redundant impact of PFAA generation and accumulation on soil key functions. Even in a closed system where PFAA accumulate, overall soil productivity was not significantly impacted in the contaminated samples, as the known functional redundancy of the soil microbial community is likely capable of ensuring the continuity of these critical ecosystem services regardless of which taxa is performing such functions (Lee et al. 2023). Nevertheless, these hypotheses are based solely on abundance variations of 16S rRNA gene ASVs, which may not completely depict real dynamics and functions of the microbial community.

Among the ASVs being enriched in the contaminated samples, only the phylotypes belonging to the genera *Terrimonas*, ADurb.Bin063-1, Candidatus *Xiphinemato-*

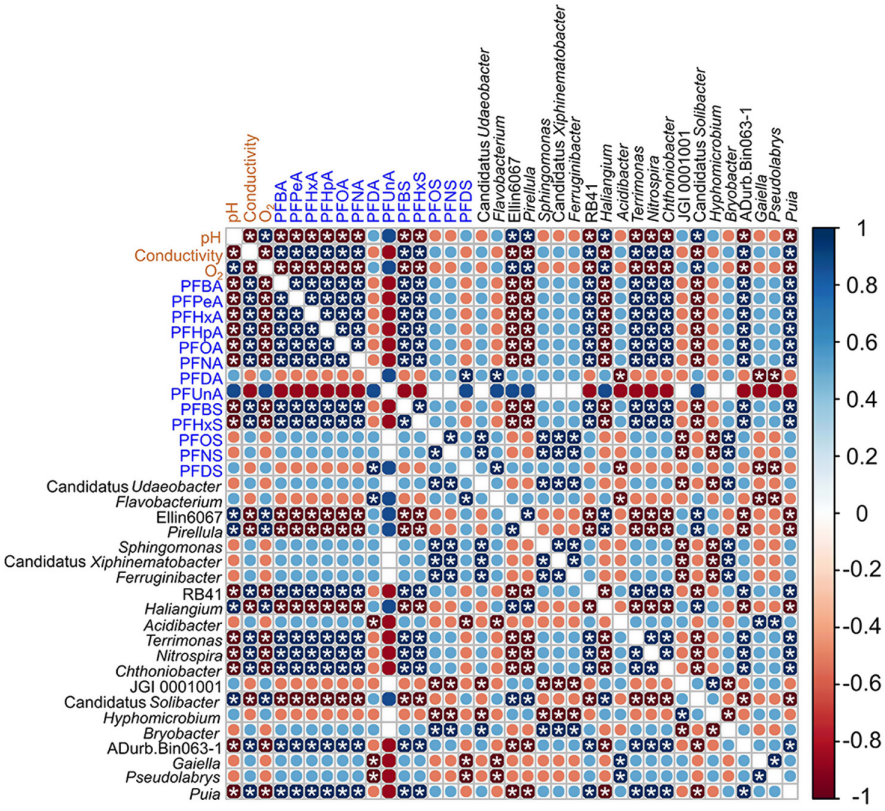

Figure 8. Spearman correlations between the predominant ASVs of contaminated samples, PFAS transformation products and physicochemical parameters. Asterisks (*) denote statistically significant ($p < 0.001$) correlations.

bacter, *Chthoniobacter*, and *Nitrospira* showed a significant positive correlation ($p < 0.001$) with one or more PFAS products (Figure 6). Interestingly, *Terrimonas*, ADurb.Bin063-1, *Chthoniobacter*, and *Nitrospira* all consistently correlated positively with PFBA, PFPeA, PFHxA, PFHpA, PFOA, PFNA, PFBS, and PFHxS (Figure 8). On the other hand, Candidatus *Xiphinematobacter* was selectively correlated only with PFOS and PFNS (Figure 8). Except for *Nitrospira*, all these phylotypes are known polysaccharide degraders. While microbial carbohydrate-active enzymes have not been directly linked to the biotransformation of PFAS precursors, it is possible that the co-utilization of monomeric sugars (derived from polysaccharide depolymerization) provides a catabolic advantage to these taxa to biotransform many of these PFAS precursors, since co-metabolic strategies seem to be the most effective route for the biotransformation of PFAA precursors (Berhanu et al. 2023).

Conclusions

Long-term assessment of PFAA generated from PFAS precursors in agricultural topsoil, leading to potential groundwater contamination, requires the quantification of generation rates and the precursor reservoir. In this work, we demonstrate that laboratory batch incubations are a good proxy for predicting field generation rates as the difference between the rate constants produced by the two methodologies were within an order of magnitude of each other. Laboratory-derived generation rates should be considered as a best-case scenario for the minimum time scale expected to achieve removal of PFAS from the field, as these rates were derived under optimal survival conditions for microorganisms (e.g., 20 °C, well mixed, complete water saturation). Consequently, these data confirmed that it would take several decades for the majority of short-chain PFAA precursors to be depleted from the BS-NRW site.

A general limitation of this study is that, besides PFCA and PFSA, other PFAS with different moieties (e.g., -SF_5 group) were under-reported in routine targeted analysis and shown to contribute to the further burden of PFAS at the site. Therefore, it is of importance at PFAS-impacted sites to extend the scope of investigation from the common target analysis of PFCA and PFSA. This includes applying other tools (e.g., dTOP or similar assays and non-target screening methods) and batch incubations to better capture the extent and time scales of the contamination.

Despite the dissimilarities observed between the microbial communities of contaminated and field control soils, the most relevant shifts detected between these microbial communities occurred at the genus level. Considering the known functional redundancy and modularity of soil microbiomes, these lower tier shifts may not translate into significant impacts in soil function and productivity; however, this requires further research. The fact that all condition-specific ASVs detected in this work correspond to bacterial phylotypes implicated in similar soil functions further reinforces this. Interestingly, apart from *Nitrospira*, all ASVs enriched in the contaminated soils and positively correlating with at least one PFAS transformation product are known poly-

saccharide degraders. This suggests a potentially relevant co-metabolic niche linked to PFAA precursor biotransformations. Still, further experimental corroboration of these microbiome dynamics would be required to ascertain these metabolic correlations.

Overall, our results demonstrate that laboratory batch tests provide a reasonable estimate of generation rates of short-chain PFAA from unknown precursors. In combination with the potential reservoir of PFAA obtained by the dTOP or similar assays, minimum time scales for PFAA release from PFAS-impacted sites may be estimated. This method can likely be applied to similar PFAS-impacted sites with precursors (e.g., AFFF sites), but further research is needed to elucidate effects of changing environmental conditions (temperature, moisture, sorption, microbial communities' composition, and activities) to improve time scale estimates of PFAS soil contaminations.

Acknowledgment

This study was funded by the state of Baden-Württemberg through Project SiWaPFC (BWPFC19001). The authors thank the NRW state EPAs (Landesamt für Natur, Umwelt und Verbraucherschutz, LANUV) for their support. K.J.T. is funded by the Excellence Strategy of the University of Tübingen (German Research Foundation [DFG], ZUK 63). D.S. acknowledges funding from the Exzellenzcluster "Controlling microbes to fight infection" (CMFI), EXC-2124. This paper has not been subjected to peer review within any of the mentioned organizations and the conclusions stated here do not necessarily reflect the official views of these organizations, nor does this document constitute an official endorsement by any of these organizations. The authors are also thankful to the University of Tübingen laboratory staff for helping to support the UPLC–MS/MS analytics; to Franziska Schädler for helping to prepare the sample for sequencing; to Bernd Susset, Jens Utermann, and Stefan Schroers for coordinating site sampling. The authors declare no conflict of interest. Open Access funding enabled and organized by Projekt DEAL.

Data Availability Statement

The data that support the findings of this study are available from the corresponding author upon reasonable request.

Supporting Information

Additional Supporting Information may be found in the online version of this article. Supporting Information is generally not peer reviewed.

Dataset S1. Metadata and ASVs collected from batch incubations (Excel© file).

Table S1. PFAS standards and internal standards used in the targeted analysis.

Table S2. Chemical structures of PFCA compounds analyzed as part of this study.

Table S3 Chemical structures of PFSA compounds analyzed as part of this study.

Table S4. Soil parameters for the contaminated topsoil.

Table S5. PFAS recovery values during soil extraction for posterior targeted analyses and dTOP.

Table S6. PFAS recovery values during soil extraction for spiked water samples.

Table S7. Mobile phase gradient used for PFAS separation.

Table S8. Mass spectrometer setting parameters.

Table S9. Parameters used during the dynamic multiple reaction monitoring (dMRM) for the different targeted compounds and their corresponding precursor and product ions, with the respective collision energies (CE) and fragmentor voltages (FV).

Table S10. O_2, pH, and electrical conductivity measurements from contaminated, field control and sterile control batch incubations.

Figure S1. Plan view of the PFAS contaminated agricultural field site in Brilon-Scharfenberg North Rhine-Westphalia (BS-NRW), Germany (51°25′39.53″N; 8°31′24.43″E), showing the six zones sampled to obtain the contaminated mixed sample.

Figure S2. Overview of the mixing procedure to homogenize soils samples starting from the master bucket for further use in batch incubation.

Figure S3. Mass percentage of PFAAs recovered in the column effluent with the contaminated topsoil until *LS* 10.

Figure S4. Changes in mean aqueous concentrations (µg/L) of perfluoroalkyl acids (PFAA) in contaminated batch incubations and sterile controls.

Figure S5. Mass (µg) of PFBA, PFPeA, PFHxA, PFHpA, PFOA, and PFBS in the aqueous phase of triplicate batch experiment samples throughout a 60 d incubation normalized to dry mass of soil (kg).

Figure S6. Cumulative (Σ) mass (kg) of PFOS, PFOA, PFBA, PFPeA, PFHxA, PFHpA, PFNA, PFDA, PFBS, and PFHxS collected during the monitoring period of August 2009 to August 2023.

Figure S7. Alpha diversity indexes calculated for individual replicates of field control and contaminated soils after 0, 28, and 60 days of incubation.

Figure S8. Taxonomic structure of the microbiomes of field control and contaminated soils after 0, 28 and 60 days of incubation (considering ASVs with at least 0.1% of relative abundance).

References

Anderson, R.H. 2021. The case for direct measures of soil-to-groundwater contaminant mass discharge at AFFF-impacted sites. *Environmental Science & Technology* 55, no. 10: 6580–6583.

Bekele, D.N., Y. Liu, M. Donaghey, A. Umeh, C.S.V. Arachchige, S. Chadalavada, and R. Naidu. 2020. Separation and lithological mapping of PFAS mixtures in the vadose zone at a contaminated site. *Frontiers in Water* 2: 597810.

Benskin, J.P., M.G. Ikonomou, F.A.P.C. Gobas, T.H. Begley, M.B. Woudneh, and J.R. Cosgrove. 2013. Biodegradation of n-ethyl perfluorooctane sulfonamido ethanol (EtFOSE) and EtFOSE-

based phosphate diester (SAmPAP diester) in marine sediments. *Environmental Science & Technology* 47, no. 3: 1381–1389.

Berhanu, A., I. Mutanda, T. Ji, M.A. Qaria, B. Yang, and D. Zhu. 2023. A review of microbial degradation of per- and polyfluoroalkyl substances (PFAS): Biotransformation routes and enzymes. *Science of the Total Environment* 859: 160010.

Bräunig, J., C. Baduel, C.M. Barnes, and J.F. Mueller. 2019. Leaching and bioavailability of selected perfluoroalkyl acids (PFAAs) from soil contaminated by firefighting activities. *Science of the Total Environment* 646: 471–479.

Bugsel, B., and C. Zwiener. 2020. LC-MS screening of poly- and perfluoroalkyl substances in contaminated soil by Kendrick mass analysis. *Analytical and Bioanalytical Chemistry* 412, no. 20: 4797–4805.

Callahan, B.J., P.J. McMurdie, M.J. Rosen, A.W. Han, A.J.A. Johnson, and S.P. Holmes. 2016. DADA2: High-resolution sample inference from Illumina amplicon data. *Nature Methods* 13, no. 7: 581–583.

Cao, Y., Q. Dong, D. Wang, P. Zhang, Y. Liu, and C. Niu. 2022. microbiomeMarker: An R/Bioconductor package for microbiome marker identification and visualization. *Bioinformatics* 38, no. 16: 4027–4029.

Caporaso, J.G., J. Kuczynski, J. Stombaugh, K. Bittinger, F.D. Bushman, E.K. Costello, N. Fierer, A.G. Pena, J.K. Goodrich, J.I. Gordon, G.A. Huttley, S.T. Kelley, D. Knights, J.E. Koenig, R.E. Ley, C.A. Lozupone, D. McDonald, B.D. Muegge, M. Pirrung, J. Reeder, J.R. Sevinsky, P.J. Tumbaugh, W.A. Walters, J. Widmann, T. Yatsunenko, J. Zaneveld, and R. Knight. 2010. QIIME allows analysis of high-throughput community sequencing data. *Nature Methods* 7, no. 5: 335–336.

Che, S., B. Jin, Z. Liu, Y. Yu, J. Liu, and Y. Men. 2021. Structure-specific aerobic defluorination of short-chain fluorinated carboxylic acids by activated sludge communities. *Environmental Science & Technology Letters* 8, no. 8: 668–674.

Chen, H., M. Liu, G. Munoz, D. Sung Vo, S. Sauve, Y. Yao, H. Sun, and J. Liu. 2020. Fast generation of perfluoroalkyl acids from polyfluoroalkyl amine oxides in aerobic soils. *Environmental Science & Technology Letters* 7, no. 10: 714–720.

Cook, E.K., C.I. Olivares, E.H. Antell, S. Yi, A. Nickerson, Y.J. Choi, C.P. Higgins, D.L. Sedlak, and L. Alvarez-Cohen. 2022. Biological and chemical transformation of the six-carbon polyfluoroalkyl substance *n*-dimethyl ammonio propyl perfluorohexane sulfonamide (AmPr-FHxSA). *Environmental Science & Technology* 56, no. 22: 15478–15488.

D'Eon, J.C., and S.A. Mabury. 2007. Production of perfluorinated carboxylic acids (PFCAs) from the biotransformation of polyfluoroalkyl phosphate surfictants (PAPS): Exploring routes of human contamination. *Environmental Science & Technology* 41, no. 13: 4799–4805.

Di Tommaso, P., M. Chatzou, E.W. Floden, P.P. Barja, E. Palumbo, and C. Notredame. 2017. Nextflow enables reproducible computational workflows. *Nature Biotechnology* 35, no. 4: 316–319.

DIN Media Gmbh. 2009. DIN 19528: 2009-01 Elution von Feststoffen - Perkolationsverfahren zur gemeinsamen Untersuchung des Elutionsverhaltens von anorganischen und organischen Stoffen. https://www.dinmedia.de/de/norm/din-19528/104285985#:~:text=Die%20Norm%20DIN%2019528%20legt,Folgenden%20kurz%3A%20Materialien)%20fest. Accessed February 1, 2023.

Ewels, P.A., A. Peltzer, S. Fillinger, H. Patel, J. Alneberg, A. Wilm, M.U. Garcia, P. Di Tommaso, and S. Nahnsen. 2020. The nf-core framework for community-curated bioinformatics pipelines. *Nature Biotechnology* 38, no. 3: 276–278.

Fabregat-Palau, J., M. Vidal, and A. Rigol. 2022. Examining sorption of perfluoroalkyl substances (PFAS) in biochars and other carbon-rich materials. *Chemosphere* 302: 134733.

Fabregat-Palau, J., M. Vidal, and A. Rigol. 2021. Modelling the sorption behaviour of perfluoroalkyl carboxylates and perfluoroalkane sulfonates in soils. *Science of the Total Environment* 801: 149343.

Fang, Y., G. Vanzin, A.M. Cupples, and T.J. Strathmann. 2020. Influence of terminal electron-accepting conditions on the soil microbial community and degradation of organic contaminants of emerging concern. *Science of the Total Environment* 706: 135327.

Göckener, B., A. Fliedner, H. Rudel, A. Badry, and J. Koschorreck. 2022. Long-term trends of per- and polyfluoroalkyl substances (PFAS) in suspended particular matter from german rivers using the direct total oxidizable precursor (dTOP) assay. *Environmental Science & Technology* 56, no. 1: 208–217.

Grathwohl, P., and B. Susset. 2009. Comparison of percolation to batch and sequential leaching tests: Theory and data. *Waste Management* 29, no. 10: 2681–2688.

Guelfo, J.L., and C.P. Higgins. 2013. Subsurface transport potential of perfluoroalkyl acids at aqueous film-forming foam (AFFF)-impacted sites. *Environmental Science & Technology* 47, no. 9: 4164–4171.

Haluska, A.A., and K.T. Finneran. 2021. Increasing electron donor concentration does not accelerate complete microbial reductive dechlorination in contaminated sediment with native organic carbon. *Biodegradation* 32, no. 5: 577–593.

Holmes, S., and P.J. McMurdie. 2013. Phyloseq: An r package for reproducible interactive analysis and graphics of microbiome census data. *PLoS One* 8, no. 4: e61217.

Houtz, E.F., and D.L. Sedlak. 2012. Oxidative conversion as a means of detecting precursors to perfluoroalkyl acids in urban runoff. *Environmental Science & Technology* 46, no. 17: 9342–9349.

Huang, S., and P.R. Jaffe. 2019. Defluorination of perfluorooctanoic acid (PFOA) and perfluorooctane sulfonate (PFOS) by *Acidimicrobium* sp. strain a6. *Environmental Science & Technology* 53, no. 19: 11410–11419.

Jiang, T., M. Geisler, W. Zhang, and Y. Liang. 2021. Fluoroalkyl-ether compounds affect microbial community structures and abundance of nitrogen cycle-related genes in soil-microbe-plant systems. *Ecotoxicology and Environmental Safety* 228: 113033.

Joerss, H., T.-R. Schramm, L. Sun, C. Guo, J. Tang, and R. Ebinghaus. 2020. Per- and polyfluoroalkyl substances in Chinese and German river water – point source- and country-specific fingerprints including unknown precursors. *Environmental Pollution* 267: 115567.

Johnson, G.R. 2022. PFAS in soil and groundwater following historical land application of biosolids. *Water Research* 211: 118035.

Kabiri, S., W. Tucker, D.A. Navarro, J. Braunig, K. Thompson, E.R. Knight, T.M.H. Nguyen, C. Grimison, C.M. Barnes, C.P. Higgins, J.F. Mueller, R.S. Kookana, and M.J. McLaughlin. 2022. Comparing the leaching behavior of per- and polyfluoroalkyl substances from contaminated soils using static and column leaching tests. *Environmental Science & Technology* 56, no. 1: 368–378.

Kurtzer, G.M., V. Sochat, and M.W. Bauer. 2017. Singularity: Scientific containers for mobility of compute. *PLoS One* 12, no. 5: e0177459.

Lee, K.K., Y. Park, and S. Kuehn. 2023. Robustness of microbiome function. *Current Opinion in Systems Biology* 36: 100479.

Lewis, M., M.H. Kim, E.J. Liu, N. Wang, and K.-H. Chu. 2016. Biotransformation of 6:2 polyfluoroalkyl phosphates (6:2 PAPs): Effects of degradative bacteria and co-substrates. *Journal of Hazardous Materials* 320: 479–486.

Liou, J.S.C., B. Szostek, C.M. DeRito, and E.L. Madsen. 2010. Investigating the biodegradability of perfluorooctanoic acid. *Chemosphere* 80, no. 2: 176–183.

Liu, C., and J. Liu. 2016. Aerobic biotransformation of polyfluoroalkyl phosphate esters (PAPs) in soil. *Environmental Pollution* 212: 230–237.

Liu, J., and S.M. Avendano. 2013. Microbial degradation of polyfluoroalkyl chemicals in the environment: A review. *Environment International* 61: 98–114.

Liu, J., N. Wang, B. Szostek, R.C. Buck, P.K. Panciroli, P.W. Folsom, L.M. Sulecki, and C.A. Bellin. 2010. 6-2 fluorotelomer alcohol aerobic biodegradation in soil and mixed bacterial culture. *Chemosphere* 78, no. 4: 437–444.

Martin, M. 2011. Cutadapt removes adapter sequences from high-throughput sequencing reads. *EMBnet.journal* 17, no. 1: 10–12.

McLachlan, M.S., S. Felizeter, M. Klein, M. Kotthoff, and P. De Voogt. 2019. Fate of a perfluoroalkyl acid mixture in an agricultural soil studied in lysimeters. *Chemosphere* 223: 180–187.

Munoz, G., A.M. Michaud, M. Liu, S.V. Duy, D. Montenach, C. Resseguier, F. Watteau, V. Sappin-Didier, F. Feder, T. Morvan, S. Houot, M. Desrosiers, J.X. Liu, and S. Sauve. 2022. Target and nontarget screening of pfas in biosolids, composts,and other organic waste products for land application in France. *Environmental Science & Technology* 56, no. 10: 6056–6068.

Naidu, R., S. Nandy, M. Megharaj, R.P. Kumar, S. Chadalavada, Z.L. Chen, and M. Bowman. 2012. Monitored natural attenuation of a long-term petroleum hydrocarbon contaminated sites: A case study. *Biodegradation* 23, no. 6: 881–895.

Newell, C.J., D.T. Adamson, P.R. Kulkarni, B.N. Nzeribe, J.A. Connor, J. Popovic, and H.F. Stroo. 2021. Monitored natural attenuation to manage PFAS impacts to groundwater: Scientific basis. *Ground Water Monitoring and Remediation* 41, no. 4: 76–89.

Nickerson, A., A.C. Maizel, C.I. Olivares, C.E. Schaefer, and C.P. Higgins. 2021. Simulating impacts of biosparging on release and transformation of poly- and perfluorinated alkyl substances from aqueous film-forming foam-impacted soil. *Environmental Science & Technology* 55, no. 23: 15744–15753.

O'Carroll, D.M., T.C. Jeffries, M.J. Lee, S.T. Le, A. Yeung, S. Wallace, N. Battye, D.J. Patch, M.J. Manefield, and K.P. Weber. 2020. Developing a roadmap to determine per- and polyfluoroalkyl substances-microbial population interactions. *Science of the Total Environment* 712: 135994.

Otte, J.M., N. Blackwell, V. Soos, S. Rughoft, M. Maisch, A. Kappler, S. Kleindienst, and C. Schmidt. 2018. Sterilization impacts on marine sediment-are we able to inactivate microorganisms in environmental samples? *FEMS Microbiology Ecology* 94, no. 12: fiy189.

Pruesse, E., C. Quast, K. Knittel, B.M. Fuchs, W.G. Ludwig, J. Peplies, and F.O. Glockner. 2007. SILVA: A comprehensive online resource for quality checked and aligned ribosomal RNA sequence data compatible with ARB. *Nucleic Acids Research* 35, no. 21: 7188–7196.

Rayner, J.L., D. Slee, S. Falvey, R. Kookana, E. Bekele, G. Stevenson, A. Lee, and G.B. Davis. 2022. Laboratory batch representation of PFAS leaching from aged field soils: Intercomparison across new and standard approaches. *The Science of the Total Environment* 838, no. 4: 156562.

Rhoads, K.R., E.M.L. Janssen, R.G. Luthy, and C.S. Criddle. 2008. Aerobic biotransformation and fate of N-ethyl perfluorooctane sulfonamidoethanol (N-EtFOSE) in activated sludge. *Environmental Science & Technology* 42, no. 8: 2873–2878.

Röhler, K., B. Susset, and P. Grathwohl. 2023. Production of perfluoroalkyl acids (PFAAs) from precursors in contaminated agricultural soils: Batch and leaching experiments. *Science of the Total Environment* 902: 166555.

Röhler, K., A.A. Haluska, B. Susset, B. Liu, and P. Grathwohl. 2021. Long-term behavior of PFAS in contaminated agricultural soils in Germany. *Journal of Contaminant Hydrology* 241: 103812.

Schaefer, C.E., J. Hooper, M. Modiri-Gharehveran, D.M. Drennan, N. Beecher, and L. Lee. 2022. Release of poly- and perfluoroalkyl substances from finished biosolids in soil mesocosms. *Water Research* 217: 118405.

Schroers, S. 2021. RE: Probenahme in Brilon-Scharfenberg ZAG Tübingen im September [Email to Bernd Susset].

Senevirathna, S.T.M.L.D., K.C.B. Krishna, R.m. Mahinroosta, and A. Sathasivan. 2022. Comparative characterization of microbial communities that inhabit PFAS-rich contaminated sites: A case-control study. *Journal of Hazardous Materials* 423: 126941.

Sepulvado, J.G., A.C. Blaine, L.S. Hundal, and C.P. Higgins. 2011. Occurrence and fate of perfluorochemicals in soil following the land application of municipal biosolids. *Environmental Science & Technology* 45, no. 19: 8106–8112.

Sharifan, H., M. Bagheri, D. Wang, J.G. Burken, C.P. Higgins, Y. Liang, J. Liu, C.E. Schaefer, and J. Blotevogel. 2021. Fate and transport of per- and polyfluoroalkyl substances (PFASs) in the vadose zone. *Science of the Total Environment* 771: 145427.

Silva, J.A.K., W.A. Martin, J.L. Johnson, and J.E. McCray. 2019. Evaluating air-water and NAPL-water interfacial adsorption and retention of perfluorocarboxylic acids within the vadose zone. *Journal of Contaminant Hydrology* 223: 103472.

Stahl, T., R.A. Riebe, S. Falk, K. Failing, and H. Brunn. 2013. Long-term lysimeter experiment to investigate the leaching of perfluoroalkyl substances (PFASs) and the carry-over from soil to plants: Results of a pilot study. *Journal of Agricultural and Food Chemistry* 61, no. 8: 1784–1793.

Straub, D., N. Blackwell, A. Langarica-Fuentes, A. Peltzer, S. Nahnsen, and S. Kleindienst. 2020. Interpretations of environmental microbial community studies are biased by the selected 16S rRNA (gene) amplicon sequencing pipeline. *Frontiers in Microbiology* 11: 550420.

Wang, N., R.C. Buck, B. Szostek, L.M. Sulecki, and B.W. Wolstenholme. 2012. 5:3 polyfluorinated acid aerobic biotransformation in activated sludge via novel "one-carbon removal pathways.". *Chemosphere* 87, no. 5: 527–534.

Wang, N., J. Liu, R.C. Buck, S.H. Korzeniowski, B.W. Wolstenholme, P.W. Folsom, and L.M. Sulecki. 2011. 6:2 Fluorotelomer sulfonate aerobic biotransformation in activated sludge of waste water treatment plants. *Chemosphere* 82, no. 6: 853–858.

Wang, N., B. Szostek, R.C. Buck, P.W. Folsom, L.M. Sulecki, and J.T. Gannon. 2009. 8-2 Fluorotelomer alcohol aerobic soil biodegradation: Pathways, metabolites, and metabolite yields. *Chemosphere* 75, no. 8: 1089–1096.

Washington, J.W., H. Yoo, J.J. Ellington, T.M. Jenkins, and E.L. Libelo. 2010. Concentrations, distribution, and persistence of perfluoroalkylates in sludge-applied soils near Decatur, Alabama, USA. *Environmental Science & Technology* 44, no. 22: 8390–8396.

Weathers, T.S., K. Harding-Marjanovic, C.P. Higgins, L. Alvarez-Cohen, and J.O. Sharp. 2016. Perfluoroalkyl acids inhibit reductive dechlorination of trichloroethene by repressing dehalococcoides. *Environmental Science & Technology* 50, no. 1: 240–248.

Wei, T. 2021. Corrplot: Visualization of a correlation matrix. Comprehensive R Archive Network.

Wu, E., K. Wang, Z. Liu, J. Wang, H. Yan, X. Zhu, X. Zhu, and B. Chen. 2023. Metabolic and microbial profiling of soil microbial community under per- and polyfluoroalkyl substance (PFAS) stress. *Environmental Science & Technology* 57, no. 51: 21855–21865.

Yi, L., Q. Peng, D. Liu, L. Zhou, C. Tang, Y. Zhou, and L. Chai. 2019. Enhanced degradation of perfluorooctanoic acid by a genome shuffling-modified *Pseudomonas parafulva* YAB-1. *Environmental Technology* 40, no. 24: 3153–3161.

Yi, L.B., L.Y. Chai, Y. Xie, Q.J. Peng, and Q.Z. Peng. 2016. Isolation, identification, and degradation performance of a PFOA-

degrading strain. *Genetics and Molecular Research* 15, no. 2: gmr.15028043.

Yoo, H., J.W. Washington, J.J. Ellington, T.M. Jenkins, and M.P. Neill. 2010. Concentrations, distribution, and persistence of fluorotelomer alcohols in sludge-applied soils near Decatur, Alabama, USA. *Environmental Science & Technology* 44, no. 22: 8397–8402.

Zweigle, J., B. Bugsel, K. Roehler, A.A. Haluska, and C. Zwiener. 2023. PFAS-contaminated soil site in Germany: Nontarget screening before and after direct top assay by kendrick mass defect and findpfΔs. *Environmental Science & Technology* 57, no. 16: 6647–6655.

Biographical Sketches

***Alexander Arthur Haluska**, corresponding author, is at the Department of Geosciences, Universität Tübingen, Schnarrenbergstraße 94-96, 72076, Tübingen, Germany; Eberhard Karls University of Tübingen: Tübingen, Baden-Württemberg, Germany; alexander.haluska@uni-tuebingen.de [Correction added after first online publication on 1 April 2025. The additional affiliation details for the first author, Alexander Arthur Haluska, have been included: [Eberhard Karls University of Tübingen: Tübingen, Baden-Württemberg, Germany].]*

***Klaus Röhler** is at the Department of Geosciences, Universität Tübingen, Schnarrenbergstraße 94-96, 72076, Tübingen, Germany.*

***Joel Fabregat-Palau** is at the Department of Geosciences, Universität Tübingen, Schnarrenbergstraße 94-96, 72076, Tübingen, Germany.*

***Diogo Alexandrino** is at the Interdisciplinary Centre of Marine and Environmental Research (CIIMAR), University of Porto, Avenida General Norton de Matos s/n, 4450-208 Matosinhos; Department of Environmental Health, School of Health, P. Porto, R. Dr. António Bernardino de Almeida 400, 4200-072 Porto, Portugal.*

***Sergey Abramov** is at the Institute of Sanitary Engineering, Water Quality and Solid Waste Management, University of Stuttgart, Bandtäle 2, 70569 Stuttgart-Büsnau, Germany.*

***Katharine Thompson** is at the Institute of Sanitary Engineering, Water Quality and Solid Waste Management, University of Stuttgart, Bandtäle 2, 70569 Stuttgart-Büsnau, Germany.*

***Daniel Straub**, Ph.D., is at the Quantitative Biology Center (QBiC), Universität Tübingen, Senior Researcher, Tübingen 72076, Germany.*

***Sara Kleindienst** is at the Institute of Sanitary Engineering, Water Quality and Solid Waste Management, University of Stuttgart, Bandtäle 2, 70569 Stuttgart-Büsnau, Germany.*

***Boris Bugsel** is at the Department of Geosciences, Universität Tübingen, Schnarrenbergstraße 94-96, 72076, Tübingen, Germany.*

***Jonathan Zweigle** is at the Department of Geosciences, Universität Tübingen, Schnarrenbergstraße 94-96, 72076, Tübingen, Germany.*

***Christian Zwiener** is at the Department of Geosciences, Universität Tübingen, Schnarrenbergstraße 94-96, 72076, Tübingen, Germany.*

***Peter Grathwohl** is at the Department of Geosciences, Universität Tübingen, Schnarrenbergstraße 94-96, 72076, Tübingen, Germany.*